Classical and quantum-mechanical treatments of nonsequential double ionization with few-cycle laser pulses

C. Figueira de Morisson Faria,[1] X. Liu,[2] A. Sanpera,[1] and M. Lewenstein[1]
[1]*Institut für Theoretische Physik, Universität Hannover, Appelstrasse 2, 30167 Hannover, Germany*
[2]*Max-Born-Institut, Max-Born-Strasse 2A, 12489 Berlin, Germany*
(Received 18 May 2004; published 15 October 2004)

We address nonsequential double ionization induced by strong, linearly polarized laser fields of only a few cycles, considering a physical mechanism in which the second electron is dislodged by the inelastic collision of the first electron with its parent ion. The problem is treated classically, using an ensemble model, and quantum mechanically, within the strong-field and uniform saddle-point approximations. In the latter case, the results are interpreted in terms of "quantum orbits," which can be related to the trajectories of a classical electron in an electric field. We obtain highly asymmetric electron momentum distributions, which strongly depend on the absolute phase, i.e., on the phase difference between the pulse envelope and its carrier frequency. Around a particular value of this parameter, the distributions shift from the region of positive to that of negative momenta, or vice versa, in a radical fashion. This behavior is investigated in detail for several driving-field parameters, and provides a very efficient method for measuring the absolute phase. Both models yield very similar distributions, which share the same physical explanation. There exist, however, minor discrepancies due to the fact that, beyond the region for which electron-impact ionization is classically allowed, the yields from the quantum-mechanical computation decay exponentially, whereas their classical counterparts vanish.

DOI: 10.1103/PhysRevA.70.043406 PACS number(s): 32.80.Rm, 32.80.Qk

I. INTRODUCTION

Linearly polarized laser pulses of intensities higher than 10^{14} W/cm^2 and only a few cycles are of vital importance to several areas of physics, being applicable to, for instance, solid-state physics [1], high-frequency sources [2], or isolated attosecond pulses [3]. Only the latter application led to a breakthrough in metrology, making it possible to trace the motion of bound electrons [4], to probe molecular dynamics [5], and to control electron emission [6]. In this pulse-length regime, the phase difference between the pulse envelope and its carrier frequency, known as "absolute phase," has a major influence on strong-field optical phenomena, such as high-order harmonic generation (HHG) [7] or above-threshold ionization (ATI) [8]. In particular, the absolute phase affects, for instance, the harmonic or photoelectron yields, the maximal energies in both spectra, and the time profiles of ATI and HHG. This is a direct consequence of the physical mechanisms governing such phenomena, which occur in a subfemtosecond time scale, and for which the time dependence of the electric field is important. In fact, high-order harmonic generation is the outcome of a three-step process in which an electron leaves an atom by tunneling ionization at a time t', propagates in the continuum, and recombines with its parent ion at a later instant t, releasing the energy gained from the field in the form of high-frequency radiation. A similar mechanism is also responsible for ATI, with the main difference that the electron either rescatters elastically with its parent ion or reaches the detector without recolliding, originating high- or low-energy peaks in the spectra, respectively. Such a mechanism has been extensively studied both classically [9,10] and quantum mechanically [11].

From the experimental point of view, controlling or measuring the absolute phase is a very difficult task [13]. This has led to the proposal and experimental realization of schemes for its diagnosis, such as, for instance, using the asymmetry in ATI photoelectron counts reaching two opposite detectors placed in a plane perpendicular to the laser field [12].

Another phenomenon whose physical explanation lies on a laser-assisted rescattering process is nonsequential double ionization (NSDI). In this case, an electron recollides inelastically with its parent ion, giving part of its kinetic energy to a second electron, which is thus able to overcome the second ionization potential and reach the continuum. Fingerprints of such a mechanism were only revealed very recently, in experiments in which the momentum component parallel to the laser field polarization could be resolved, either for the doubly charged ion [14] or for both electrons [15]. Such features, namely a doubly peaked structure in the momentum distributions, with maxima at $p_{1\|}=p_{2\|}=\pm 2\sqrt{U_p}$, where $p_{j\|}(j=1,2)$ and U_p denote the electron momentum components parallel to the laser field polarization and the ponderomotive energy [16], respectively, are, up to the present date, the most striking example of electron-electron correlation in the context of atoms in strong laser fields. This fact has led not only to further experiments [17], but also to considerable theoretical activity on the subject, using quantum-mechanical [18–22], semiclassical [23–26], and classical [27–29] methods.

Recently, we have shown that NSDI may serve as a powerful tool for absolute-phase measurements, exploiting the fact that, for few-cycle driving pulses, inversion symmetry is broken [29]. Thus, the distributions in $(p_{1\|},p_{2\|})$ are mainly concentrated in the positive or negative momentum regions, changing from one region to the other upon a critical phase. Such investigations have been performed classically, considering electrons released at times t' uniformly distributed

throughout the pulse and weighted with the quasistatic tunneling rate [30].

In this paper, we deal with this problem quantum mechanically, and investigate the existence of a one-to-one correspondence with the classical model in Ref. [29]. Similar studies have been performed for NSDI with monochromatic driving fields, with practically identical outcomes [25,26]. This has shown that, at least in the monochromatic case, which is a good approximation for the long pulses used in the experiments, intrinsically quantum mechanical effects such as interference processes, or wave-packet spreading, are not important. However, it is legitimate to ask the question of whether this situation will persist in the few-cycle regime. Indeed, it may well be that interference and wave-packet spreading play a more important role in this latter case. Additionally, it is not clear whether the quasistatic tunneling rate considered in the classical model remains valid for few-cycle driving pulses. In fact, this has been recently called into question, with the derivation of a nonadiabatic rate [31]. Finally, it is worthwhile to check whether asymmetric distributions and the critical phase also occur in a quantum-mechanical context, and, in case they do, to understand the physics behind such features.

In particular, we address the above-stated questions using on *S*-matrix formalism, within the strong-field approximation (SFA) [32,33]. We consider the simplest type of rescattering, namely electron-impact ionization, and treat the problem in terms of the so-called "quantum orbits" [34], which appear in the context of saddle-point approximations. Specifically, we use a uniform approximation whose only validity requirement is that the orbits in question occur in pairs, which is in general the case for laser-assisted rescattering phenomena. This method has been previously applied to NSDI in monochromatic driving fields, in order to analyze the influence of the types of interaction and final-state electron-electron correlation on the yields [25,26]. Apart from considerably simplifying the computations involved, as compared to other theoretical methods [18–20], the quantum-orbit approach provides additional physical insight, in terms of a space-time picture. In fact, the quantum orbits are closely related to the orbits of a classical electron in an external laser field. Hence, in several situations, it is possible to draw a parallel betweeen our quantum-mechanical treatment and the previous classical considerations [29], discussing their similarities and differences. In the following, we study the physical mechanisms responsible for the critical phase within a quantum-mechanical framework, concentrating on the main differences from the classical picture and from the monochromatic-driving field case.

The paper is organized as follows. In the next section (Sec. II), we provide the necessary theoretical background, presenting the transition amplitude in the strong-field and uniform approximations. Subsequently, in Sec. III, we present differential electron momentum distributions for various absolute phases, discussing the main features obtained in terms of quantum orbits. The quantum-mechanical results are then compared to a classical ensemble computation which is either the same as in [29], or slightly modified with respect to it (Sec. IV). Finally, in Sec. V, we summarize the paper and state our conclusions.

II. BACKGROUND

The transition amplitude of the laser-assisted inelastic rescattering process responsible for NSDI, in the strong-field approximation [32,33], is given by

$$M = -\int_{-\infty}^{\infty} dt \int_{-\infty}^{t} dt' \langle \psi_{p_1,p_2}^{(V)}(t) | V_{12} U_1^{(V)}(t,t') V \otimes U_2^{(0)}(t,t') \times |\psi_0(t')\rangle, \tag{1}$$

where V, $U_n^{(0)}(t,t')$, $U_n^{(V)}(t,t')$, and V_{12} denote the atomic binding potential, the field-free and the Volkov time evolution operators acting on the nth ($n=1,2$) electron, and the interaction through which the second electron is freed by the first, respectively. Equation (1) expresses the following physical process: Initially, both electrons are bound, and the atom is in the ground state, which is approximated by $|\psi_0(t')\rangle = |\psi_0^{(1)}(t')\rangle \otimes |\psi_0^{(2)}(t')\rangle$ (i.e., product state of one-electron ground states), with $|\psi_0^{(n)}(t')\rangle = e^{i|E_{0n}|t'} |\psi_0^{(n)}\rangle$. At the time t', the first electron is released through tunneling ionization, whereas the second electron remains bound. Subsequently, the first electron propagates in the continuum from t' to t, gaining energy from the field. At this latter time, it collides inelastically with its parent ion, dislodging the second electron. The final electron state is then chosen as the product state of one-electron Volkov waves, $|\psi_{p_1,p_2}^{(V)}(t)\rangle = |\psi_{p_1}^{(V)}(t)\rangle \otimes |\psi_{p_2}^{(V)}(t)\rangle$, where $\mathbf{p}_1, \mathbf{p}_2$ are the final electron momenta (for studies of correlated two-electron final states see, e.g., Refs. [18,25,26]). In Eq. (1), the interaction with the ionic potential is not taken into account. In our computations, we use the length gauge and atomic units.

Expanding $U^{(V)}(t,t')$ in terms of Volkov states, Eq. (1) reads

$$M = -\int_{-\infty}^{\infty} dt \int_{-\infty}^{t} dt' \int d^3k V_{\mathbf{p}_n \mathbf{k}} V_{\mathbf{k}0} \exp[iS(t,t',\mathbf{p}_n,\mathbf{k})], \tag{2}$$

with the action

$$S(t,t',\mathbf{p}_n,\mathbf{k}) = -\frac{1}{2}\sum_{n=1}^{2} \int_{t}^{\infty} [\mathbf{p}_n + \mathbf{A}(\tau)]^2 d\tau - \frac{1}{2}\int_{t'}^{t} [\mathbf{k} + \mathbf{A}(\tau)]^2 d\tau + |E_{01}|t' + |E_{02}|t, \tag{3}$$

where $\mathbf{A}(t)$, $\mathbf{p}_n (n=1,2)$, $\mathbf{k}$, and $|E_{0n}|$ denote the vector potential, the final momenta of both electrons, the intermediate momentum of the first electron, and the ionization potentials, respectively. All the influence of the binding potential V and of the electron-electron interaction V_{12} is included in the form factors

$$V_{\mathbf{p}_n \mathrm{k}} = \langle \mathbf{p}_{n2} + \mathbf{A}(t), \mathbf{p}_1 + \mathbf{A}(t) | V_{12} | \mathbf{k} + \mathbf{A}(t), \psi_0^{(2)} \rangle \tag{4}$$

and

$$V_{\mathbf{k}0} = \langle \mathbf{k} + \mathbf{A}(t') | V | \psi_0^{(1)} \rangle \tag{5}$$

In this paper, we consider a contact-type interaction

$$V_{12} = \delta(\mathbf{r}_1 - \mathbf{r}_2)\,\delta(\mathbf{r}_2), \tag{6}$$

which yields very good agreement with experimental data within the context of NSDI in monochromatic driving fields [23,25]. In this case, the form factors $V_{\mathbf{p}_n\mathbf{k}}, V_{\mathbf{k}0}$ are constant and the SFA transition amplitude can be solved analytically up to one quadrature. For other types of potentials, this is only possible by evaluating multiple integrals numerically.

For low enough frequencies and high enough laser intensities, Eq. (2) can be solved to a good approximation by the steepest-descent method. Thus, we must determine $\mathbf{k}$, t', and t, such that $S(t,t',\mathbf{p}_n,\mathbf{k})$ is stationary, i.e., its partial derivatives with respect to these parameters vanish. This condition yields

$$[\mathbf{k} + \mathbf{A}(t')]^2 = -2|E_{01}|, \tag{7}$$

$$\sum_{n=1}^{2} [\mathbf{p}_n + \mathbf{A}(t)]^2 = [\mathbf{k} + \mathbf{A}(t)]^2 - 2|E_{02}|, \tag{8}$$

and

$$\int_{t'}^{t} d\tau [\mathbf{k} + \mathbf{A}(\tau)] = 0. \tag{9}$$

Equations (7) and (8) give the energy conservation at the start and rescattering times, respectively, while Eq. (9) constraints the intermediate momentum of the first electron so that it returns to its parent ion. For vanishing $|E_{01}|$, the classical equations of motion of both electrons in the external field are obtained. For nonzero $|E_{01}|$, Eq. (7) expresses tunneling ionization at t', and has no real solution. Physically, this means that this process is not classically allowed. This results in complex variables t', t, and $\mathbf{k}$, which always occur in pairs. The real parts of such variables are directly related to a longer and a shorter orbit of a classical electron in an electric field. The longer orbit can be associated to the so-called "slow-down collisions," which have recently been discussed in the literature [22,24,28]. The imaginary parts determine to which extent electron-impact ionization is allowed or forbidden, both within and beyond the boundaries of the classically allowed energy region. In this latter domain, one of the orbits leads to exponentially decaying contributions in the transition amplitude (2), which cause cutoffs in the distributions, while the remaining orbit starts to yield diverging contributions, and must be discarded.

Equation (8) can also be written in terms of the momentum components parallel and perpendicular to the laser-field polarization, denoted by $p_{n\parallel}$ and $\mathbf{p}_{n\perp}(n=1,2)$, respectively. In this case, for constant transverse momenta, one obtains the equation

$$\sum_{n=1}^{2} [p_{n\parallel} + A(t)]^2 = [\mathbf{k} + \mathbf{A}(t)]^2 - 2|E_{02}| - \sum_{n=1}^{2} \mathbf{p}_{n\perp}^2, \tag{10}$$

describing a circle in the $p_{1\parallel}$, $p_{2\parallel}$ plane, whose radius depends on the kinetic energy $E_{\mathrm{ret}}(t)=[\mathbf{k}+\mathbf{A}(t)]^2/2$ of the first electron upon return, and on the effective binding energy $|\tilde{E}_{02}| = |E_{02}| + \Sigma_{n=1}^{2}\mathbf{p}_{n\perp}^2/2$. If $E_{\mathrm{ret}}(t) \leqslant |\tilde{E}_{02}|$, this radius collapses and electron-impact ionization becomes classically forbidden. This means that there is not only a maximal, but also a minimal classically allowed energy, and the resulting yields exhibit two cutoffs, or no cutoff at all. This is a major difference with respect to high-order harmonic generation or above-threshold ionization, for which only maximal classically allowed energies exist.

In the standard saddle-point method, the action (3) is expanded quadratically around the saddle points, and the transition amplitude (2) is approximated by

$$M^{(\mathrm{SPA})} = \sum_s A_s \exp(iS_s), \tag{11}$$

$$S_s = S_{\mathbf{p}}(t_s, t_s', \mathbf{k}_s), \tag{12}$$

$$A_s = (2\pi i)^{5/2} \frac{V_{\mathbf{p}\mathbf{k}_s} V_{\mathbf{k}_s 0}}{\sqrt{\det S''_{\mathbf{p}}(t,t',\mathbf{k})_s}}, \tag{13}$$

where the index s runs over the relevant saddle points, and $S''_{\mathbf{p}}$ denotes the five-dimensional matrix of the second derivatives of the action with respect to t, t', and $\mathbf{k}$. In practice, we first determine $\mathbf{k}(t,t')$ as a function of the other variables, inserting this in the action, and take

$$A_s = (2\pi i)^{5/2} \frac{V_{\mathbf{p}\mathbf{k}_s} V_{\mathbf{k}_s 0}}{(t'-t)^{3/2}\sqrt{\det S''_{\mathbf{p}}(t,t')_s}}, \tag{14}$$

so that the computation of the determinant is simplified.

The above-stated saddle-point approximation is only applicable for well-isolated saddle points. This does not hold near the boundaries of the classically allowed region, where the pairs of saddles nearly coalesce. Furthermore, beyond such boundaries, one of the saddles yields diverging results, and must be discarded. This leads to cusps in the yield which are particularly problematic for nonsequential double ionization. A detailed analysis of this problem is given in [24].

Such artifacts can be eliminated by using a more general, uniform approximation [37], whose only validity requirement is that the saddles occur in pairs. This approximation has been successfully applied in the context of above-threshold ionization [36] and nonsequential double ionization [24,26].

Within this improved approximation, in the classically allowed region, the transition amplitude for a pair of trajectories i and j is given by

$$M_{i+j} = \sqrt{2\pi\Delta S/3}\,\exp(i\overline{S} + i\pi/4)\{\overline{A}[J_{1/3}(\Delta S) + J_{-1/3}(\Delta S)] + \Delta A[J_{2/3}(\Delta S) - J_{-2/3}(\Delta S)]\},$$

$$\Delta S = (S_i - S_j)/2, \quad \overline{S} = (S_i + S_j)/2,$$

$$\Delta A = (A_i - iA_j)/2, \quad \overline{A} = (iA_i - A_j)/2. \tag{15}$$

The saddle-point approximation is recovered for large values of ΔS, using the asymptotic behavior

$$J_{\pm\nu}(z) \sim \left(\frac{2}{\pi z}\right)^{1/2} \cos(z \mp \nu\pi/2 - \pi/4) \tag{16}$$

of the Bessel functions for large z. One should note that the uniform approximation considers the collective contribution of a pair of saddle points, instead of, as in the former case, taking them into account individually.

In the classically forbidden region, one of the saddles must be discarded. For that purpose, a branch of the Bessel function must be chosen in such a way that the approximation exhibits a smooth functional behavior at the Stokes transition [35], given by

$$\mathrm{Re}\ S_{\mathbf{p}}(t_i,t_i',\mathbf{k}_i) = \mathrm{Re}\ S_{\mathbf{p}}(t_j,t_j',\mathbf{k}_j). \tag{17}$$

Beyond the Stokes transition,

$$M_{i+j} = \sqrt{2i\Delta S/\pi}\ \exp(i\overline{S})[\overline{A}K_{1/3}(-i\Delta S) + i\Delta A K_{2/3}(-i\Delta S)]. \tag{18}$$

The saddle-point approximation is, again, recovered using the asymptotic expansion

$$K_\nu(z) \sim \left(\frac{\pi}{2z}\right)^{1/2} \exp(-z) \tag{19}$$

for large z. Inserting Eq. (19) into Eq. (18), it is easy to show that only one saddle contributes to the saddle-point approximation in this energy region. Equations (15) and (18) should be matched at the Stokes transitions, whose energy positions roughly coincide with the boundary between the classically allowed and forbidden energy regions.

In the following, we take the few-cycle pulse $\mathbf{E}(t) = -d\mathbf{A}(t)/dt$, with

$$\mathbf{A}(t) = A_0 \exp[-4(\omega t - \pi n)^2/(\pi n)^2]\sin[\omega t + \phi]\hat{e}_x, \tag{20}$$

where n, ω, A_0, and ϕ denote its number of cycles, frequency, amplitude, and absolute phase, respectively. We then find the start and return times such that the saddle-point equations are fulfilled, and use such times to compute the yields, which are given by

$$\Gamma(p_{1\parallel},p_{2\parallel}) = \int d^2p_{1\perp} \int d^2p_{2\perp} |M|^2, \tag{21}$$

where M is given by Eq. (2) within the uniform approximation.

III. QUANTUM-ORBIT ANALYSIS

In Fig. 1, we present the momentum distributions computed using the above-discussed method, for various absolute phases, in the form of contour plots in the $(p_{1\parallel},p_{2\parallel})$ plane. We choose the atomic species to be neon, for which electron-impact ionization is the dominant physical mechanism [38]. In general, such distributions exhibit circular shapes, centered at particular momenta along $p_{1\parallel}=p_{2\parallel}=p_\parallel$, and, in contrast to the monochromatic-field case, are no longer symmetric with respect to $(p_{1\parallel},p_{2\parallel}) \leftrightarrow (-p_{1\parallel},-p_{2\parallel})$. This symmetry breaking is expected, since the relation $A(t) = -A(t \pm T/2)$, and thus $|M(t,t',p_{1\parallel},p_{2\parallel})| = |M(t \pm T/2, t' \pm T/2, -p_{1\parallel},-p_{2\parallel})|$, which was true for monochromatic driving fields, does not hold. The circular shapes are typical for the contact-type interaction, and are also observed in the monochromatic case.

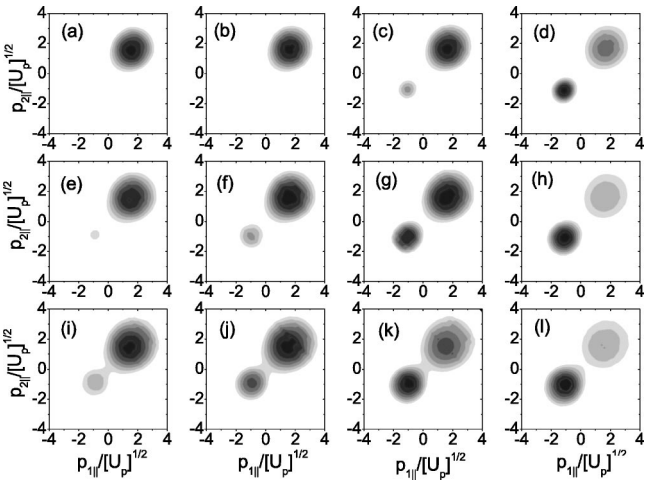

FIG. 1. Differential electron momentum distributions computed for neon ($|E_{01}|=0.79$ a.u. and $|E_{02}|=1.51$ a.u.) subject to a four-cycle pulse ($n=4$) of freqency $\omega=0.057$ a.u. and various intensities and absolute phases. The upper, middle and lower panels correspond to $I=4\times10^{14}$ W/cm^2 ($U_p=0.879$ a.u.), $I=5.5\times10^{14}$ W/cm^2 ($U_p=1.2$ a.u.), and $I=8\times10^{14}$ W/cm^2 ($U_p=1.758$ a.u.), respectively. The absolute phases are given as follows: Panels (a), (e), and (i): $\phi=0.8\pi$; panels (b), (f), and (j): $\phi=0.9\pi$; panels (c), (g), and (k): $\phi=1\pi$; and panels (d), (h), and (l): $\phi=1.1\pi$.

Depending on the phase, the yields are mainly concentrated either in the regions of positive or negative parallel momenta. For instance, in the figure, initially, the parallel momenta of both electrons are essentially positive [Figs. 1(a), 1(e), and 1(i)]. As the phase increases, contributions from negative momenta are also present, becoming more and more significant, until the distributions are almost entirely shifted from the positive to the negative momentum region [cf. Figs. 1(d), 1(h), and 1(l)]. This process occurs for different intervals of absolute phases, depending on the peak intensity of the driving field. For the specific example presented, the higher the intensity is, the earlier the momenta start to change sign.

This phase dependence is very similar to that in [29], obtained within a classical framework. Thereby, this behavior was traced back to sets of electron trajectories, whose relevance was determined by the phase space and by the rate with which the first electron was ejected in the continuum. A critical phase was related to a change in the dominant pair of orbits, which had a huge repercussion in the distributions. This phase was also shifted towards smaller absolute values with increasing driving-field intensity.

Subsequently, we analyze both the asymmetry and the critical phase in terms of pairs of quantum orbits, which are classified as $(i,j)_{(\phi)}$ according to increasing start times and absolute phases. We consider only relatively short orbits so that $t-t' \lesssim T$, where $T=2\pi/\omega$ denotes the field cycle. Longer orbits yield negligible contributions due to wave-packet spreading.

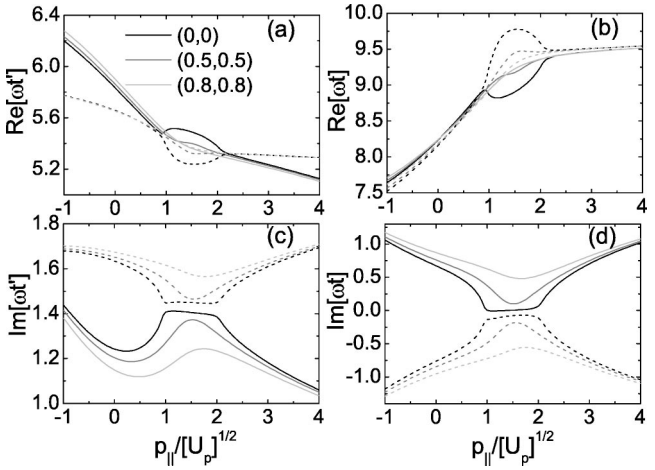

FIG. 2. Real and imaginary parts of the start and return times for the orbits 1 and 2 as functions of the parallel momentum $p_{\parallel}$ along the diagonal $p_{1\parallel}=p_{2\parallel}$, computed for a four-cycle pulse ($n=4$) of absolute phase $\phi=0.5\pi$. The atomic parameters were taken as $|E_{01}|=0.79$ a.u. and $|E_{02}|=1.51$ a.u. and correspond to neon, while the field intensity and frequency were chosen as $I=5.5\times10^{14}$ W/cm^2 ($U_p=1.2$ a.u.) and $\omega=0.057$ a.u., respectively. The numbers in the figure denote the transverse momenta ($p_{1\perp},p_{2\perp}$) in units of $\sqrt{U_p}$. The shorter and longer orbits in each pair correspond to the solid and dashed lines, respectively.

Figure 2 shows one of such pairs for t' near T, which we specifically denote $(1,2)_{(0.5\pi)}$. We consider the intermediate intensity in Fig. 1, for which the phase chosen yields positive parallel momenta, along the diagonal $p_{1\parallel}=p_{2\parallel}=p_{\parallel}$. Panels (a) and (b) display $\mathrm{Re}[\omega t']$ and $\mathrm{Re}[\omega t]$ as functions of $p_{\parallel}$, which can be associated to the times obtained by solving the classical equations of motion of two electrons colliding inelastically in a laser field. There exists always a longer and a shorter orbit for the electron, which nearly coalesce near two particular momenta. Such momenta correspond to Stokes transitions [Eq. (17)], which, for high enough intensities, roughly coincide with the minimal and maximal classically allowed momenta [39]. These two specific momenta delimit a region that is most extensive for $\mathbf{p}_{j\perp}=0$ ($j=1,2$). As the transverse momenta increase, the effective second ionization potential $|\tilde{E}_{02}|$ also becomes larger until this region collapses. An interesting feature is that, between the Stokes transitions, the real parts of the rescattering and start times are centered around a particular value of $p_{\parallel}$, which correspond to the peak of the momentum distributions. For few-cycle pulses, this center depends on the pair of orbits, as well as on the absolute phase. For monochromatic driving fields, it lies at $p_{\parallel}=\pm2\sqrt{U_p}$ [24].

The remaining panels depict the imaginary parts of such times, which provide in some sense a measure for a process being classically allowed or forbidden. Indeed, they determine whether the transition amplitudes (2) increase or decrease exponentially, or how relevant the contributions from particular sets of orbits are. These imaginary parts noticeably increase at and beyond the Stokes transitions, and remain practically constant in the momentum region in between. This suggests that, in this region, electron-impact ionization

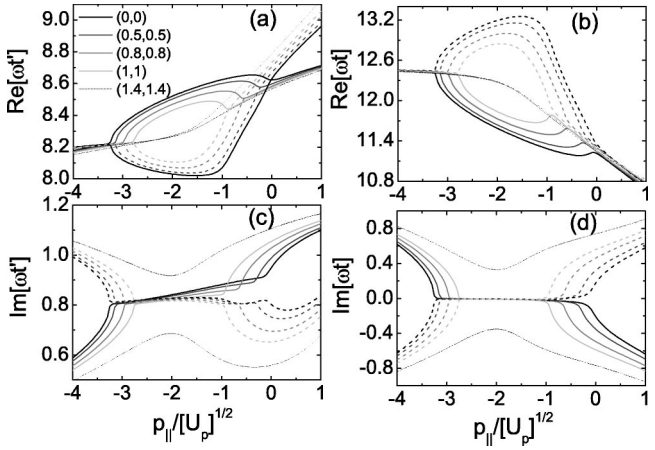

FIG. 3. The same as in the previous figures for the orbits 3 and 4.

is either classically allowed or at least much more probable to occur. Additionally, whereas $\mathrm{Im}[\omega t]$ almost vanishes in this region, $\mathrm{Im}[\omega t']$ has a nearly constant and nonvanishing value [cf. panels (c)]. This is due to the fact that tunneling *per se* is classically forbidden. Indeed, the larger this value is, the smaller is the probability that this process takes place at all.

Two additional pairs of orbits, for which $1.5T\lesssim t'\lesssim2T$, are displayed in Figs. 3 and 4. At these times, the pulse (20) is closer to its peak intensity. In such figures, there exist extensive regions between the Stokes transitions, in which $\mathrm{Re}[\omega t']$ and $\mathrm{Re}[\omega t]$ practically coincide with the start and return times obtained within a classical framework, and in which $|\mathrm{Im}[\omega t]|$ are vanishingly small. Such features are clear evidence that, in this case, electron-impact ionization is classically allowed.

Another noteworthy feature is that, in the classically allowed region, $|\mathrm{Im}[\omega t']|$ has much smaller values than those in Fig. 2. Physically, this means that the first electron left with a larger tunneling probability at t', in comparison to the orbits $(1.2)_{(0.5\pi)}$. Furthermore, the fact that this region is extensive shows that the kinetic energy of the first electron upon return is larger for $(3,4)_{(0.5\pi)}$ and $(5,6)_{(0.5\pi)}$ than for

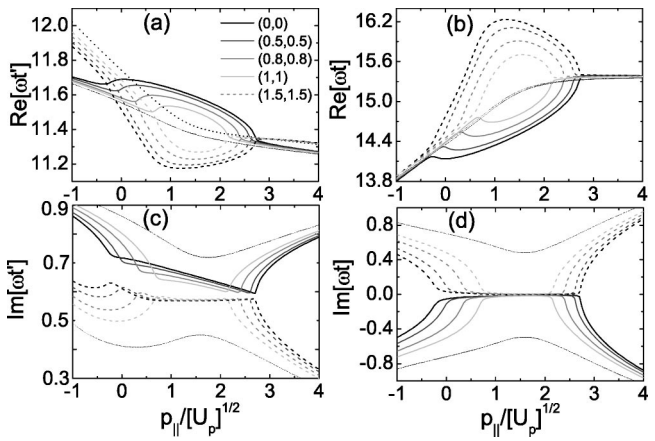

FIG. 4. The same as in the previous figures for the orbits 5 and 6.

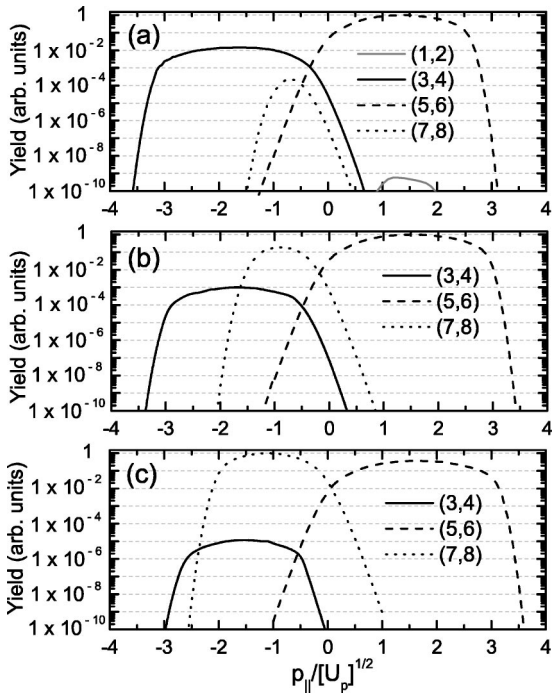

FIG. 5. Individual contributions of the four most relevant pairs of orbits to the NSDI yield, for $p_{1\|}=p_{2\|}=p_{\|}$, for ponderomotive energy $U_p=1.2$ a.u and absolute phases $\phi=0.5\pi$, $\phi=0.8\pi$, and $\phi=1.1\pi$ [panels (a), (b), and (c), respectively]. The remaining parameters are the same as in the previous figures. The curves have been normalized to the maximum of the most relevant contributions. Specifically, in panels (b) and (c), the contributions from (1,2) are smaller than the range of orders of magnitude displayed.

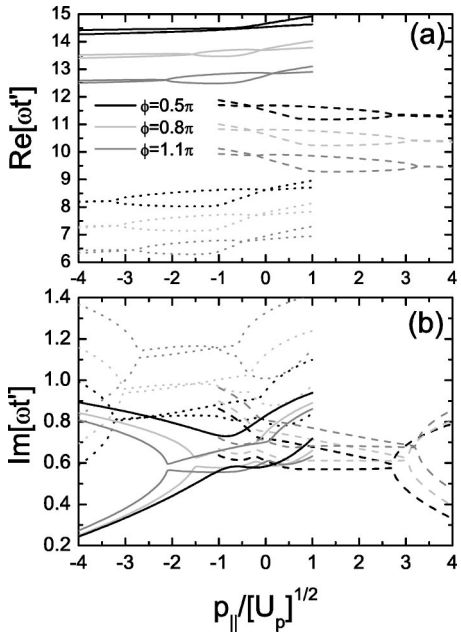

FIG. 6. Real [panel (a)] and imaginary [panel (b)] parts of the start times for the orbits (3,4), (5,6), and (7,8) along $p_{1\|}=p_{2\|}$ and for vanishing transverse momenta, indicated by dotted, dashed, and solid lines, respectively. We consider neon subject to a four-cycle ($n=4$) pulse of intensity $I=5.5\times10^{14}$ W/cm^2, various absolute phases, and frequency $\omega=0.057$ a.u. Specifically, for $\phi=0.5\pi$, electron-impact ionization is classically forbidden for the orbits (7,8).

$(1.2)_{(0.5\pi)}$. For that reason, the contributions from $(3,4)_{(0.5\pi)}$ and $(5,6)_{(0.5\pi)}$ to the total yield should be more relevant than those from $(1.2)_{(0.5\pi)}$.

This is confirmed by Fig. 5, which depicts the yields computed from each pair of the above-discussed orbits, along the diagonal $p_{1\|}=p_{2\|}=p_{\|}$. In Fig. 5(a), the contributions from $(5,6)_{(0.5\pi)}$ are at least two orders of magnitude larger than those from the remaining pairs, so that the distributions will be concentrated in the first quadrant of the $(p_{1\|},p_{2\|})$ plane. Hence, for practical purposes, the remaining contributions can be neglected. They are, however, very useful for the physical understanding of the problem.

The second most prominent contributions come from $(3,4)_{(0.5\pi)}$. This is expected, since, for these orbits, there is a relatively large probability that the first electron tunnels out, as well as a large momentum region for which electron-impact ionization is allowed.

Additional contributions come from the orbits $(1,2)_{(0.5\pi)}$ and $(7,8)_{(0.5\pi)}$. The latter set of orbits is not displayed in the previous figures, due to the fact that, in this case, there are no Stokes transitions, i.e., electron-impact ionization is forbidden throughout. Interestingly, the contributions from all pairs of orbits discussed above, including $(7,8)_{(0.5\pi)}$, are several orders of magnitude larger than those from the pair $(1,2)_{(0.5\pi)}$. This is due to the fact that, for $(7,8)_{(0.5\pi)}$, the tunneling probability for the first electron is considerably larger than for $(1,2)_{(0.5\pi)}$. From the technical viewpoint, it is worth mentioning that, for $(7,8)_{(0.5\pi)}$, the yield has been computed by using Eq. (11), and taking the orbit for which this expression is exponentially decaying.

For other absolute phases, there may be other sets of orbits whose contributions may compete with or even overwhelm those from (5,6). This is in fact the case in Figs. 5(b) and 5(c), for $\phi=0.8\pi$ and $\phi=1.1\pi$, respectively. Such phases, as well as the remaining parameters, are the same as in Figs. 1(d) and 1(f), corresponding to the beginning and to the end of a shift in the momentum distributions.

In Fig. 5(b), one clearly sees that the second most relevant pair of orbits is no longer $(3,4)_{(0.8\pi)}$, but $(7,8)_{(0.8\pi)}$. The contributions from such orbits now are only one order of magnitude smaller than those from $(5,6)_{(0.8\pi)}$. Consequently, there are also small, but not negligible, contributions in negative momentum regions. This is in agreement with Fig. 1(d), for which there is a small spot in the third quadrant of the $(p_{1\|},p_{2\|})$ plane, in addition to the dominant contributions in the first quadrant. For larger phases, such as, for instance, $\phi=1.1\pi$ [Fig. 5(c)], the contributions from (7,8) become even more relevant than those from (5,6). Hence, the distributions are shifted from the first to the third quadrant, in accordance with Fig. 1(h).

In Fig. 6, we systematically analyze the dependence of the real and imaginary parts of the times t' on the absolute phase, for the three most relevant sets of orbits. As an overall feature, for the pair (3,4) $|\mathrm{Im}[\omega t']|$ is larger than for the remaining two pairs. Physically, this means that tunneling is

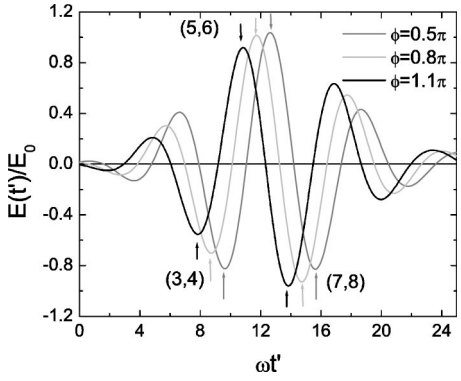

FIG. 7. Time-dependent electric field, for various absolute phases. The peak-field times are marked with arrows and the corresponding pairs of orbits are indicated by the numbers in the figure. The remaining parameters are the same as in the previous figure.

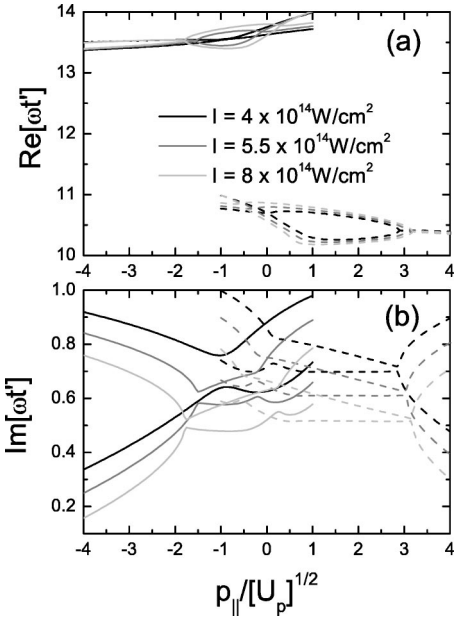

FIG. 8. Real [panel (a)] and imaginary [panel (b)] parts of the start times for the orbits (5,6),(7,8), indicated by dashed and solid lines, respectively, for absolute phase $\phi=0.8\pi$ and various laser intensities, along $p_{1\parallel}=p_{2\parallel}$ and vanishing transverse momenta. The remaining parameters are the same as in the previous figure.

less probable in this case. In general, this makes the contributions from this pair to the yield less relevant than those from the other two sets. An exception, however, occurs for $\phi=0.5\pi$, due to the fact that, in this case, electron-impact ionization is forbidden for (7,8). This leads to exponentially decaying contributions for this pair, which are overwhelmed by those from (3,4). Still, even in this particular case, these latter are two orders of magnitude smaller than the yield from the orbits (5,6) [cf. Fig. 5(a)].

For high driving-field intensities, as those in the lower panels in Fig. 1, there may exist minor, though not negligible, contributions from (3,4). In general, however, these contributions are vanishingly small. An interesting feature is that, with increasing absolute phases, this set of orbits gradually loses relevance, since $|\mathrm{Im}[\omega t']|$ increases. This can be explicitly seen in Fig. 5, where the yield from (3,4) decreases in at least three orders of magnitude as ϕ increases.

The other two pairs of orbits, (5,6) and (7,8), are, in fact, far more important to the yield. Thereby, three distinct behaviors can be identified. Below $\phi=0.8\pi$, the distributions are mainly determined by the orbits (5,6), whose contributions lie in the region of $p_{\parallel}>0$. Around this phase, the pair $(7,8)_{(0.8\pi)}$ comes into play. Indeed, although this pair does not delimit a large classically allowed region, the imaginary parts of the corresponding start times are comparable to or smaller than those of (5,6). Thus, the contributions from both pairs start to compete, and the distributions spread over both positive and negative momentum regions. As the phase increases, $|\mathrm{Im}[\omega t']|$ gradually decreases for this latter set, until the negative parallel momenta are favored. This explains the features in Fig. 1. One may refer to $\phi=0.8\pi$ as a critical phase ϕ_c, since it marks a change in the sets of dominant orbits.

The pulse profile (Fig. 7), together with the real parts of the tunneling times, allows an intuitive interpretation of the above statements. Below $\phi_c=0.8\pi$, the peak value of the pulse is near $\mathrm{Re}[\omega t']$ for the orbits (5,6), whose contributions then dominate. Thus, the distributions essentially concentrate in the positive momentum region. Around this phase, this picture starts to change, and there are two sets of orbits, namely (5,6) and (7,8), for which the instantaneous electric fields at the tunneling times are comparable. This situation persists within a phase interval until, finally, the absolute maximum of the field corresponds to the latter set of orbits, so that the momenta are mainly negative. An interesting situation occurs for $\phi=0.5\pi$, for which, in principle, there exist two sets of times near which the electric field exhibits comparable maxima, corresponding to (3,4) and (7,8). For low intensities, rescattering is not allowed for the orbits (7,8), and the contributions to the yield are absent. For high intensities, however, electron-impact ionization is already allowed in this case, so that the critical phase is shifted towards smaller values.

In Fig. 8, we explicitly show how electron-impact ionization becomes classically allowed or forbidden upon a change in the driving-field intensity, for $\phi_c=0.8\pi$. In fact, as the intensity is decreased, this process ceases to be allowed for the orbits (7,8), whose contributions lie near the peak of the pulse (cf. Fig. 7). As a direct consequence, the critical phase is shifted towards larger absolute values as the intensity decreases, as shown in Fig. 1.

IV. COMPARISON WITH CLASSICAL MODELS

In this section, we will recall and apply the classical model used in [29], performing a direct comparison with the results of the *S*-matrix computation. We consider an electron ensemble subject to the few-cycle pulse (20), which is released from the origin of the coordinate system with initial vanishing drift velocities, i.e.,

$$\mathbf{p}+\mathbf{A}(t')=0. \tag{22}$$

The varying parameters are the tunneling times t', uniformly distributed throughout the pulse, and the quasistatic tunneling rate [30]

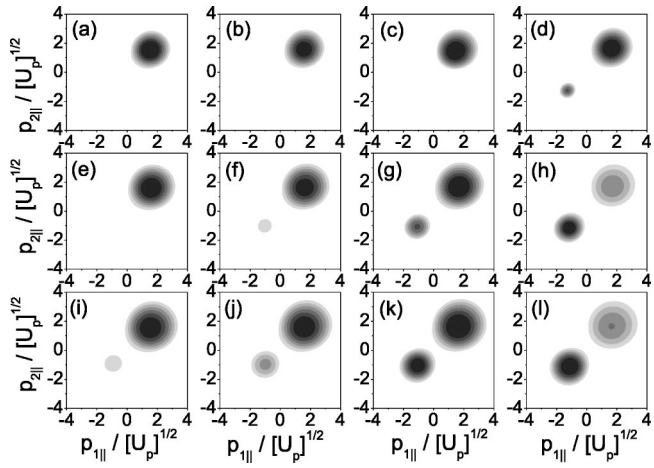

FIG. 9. Differential electron momentum distributions for the same parameters as in Fig. 1, computed with the classical model discussed in Sec. IV.

$$R(t') \sim \exp[-2(2|E_{01}|)^{3/2}/3|E(t')|]/|E(t')|, \qquad (23)$$

with which the electron counts are weighted. Some of these electrons subsequently return to the origin and free a second electron ensemble at later times t through electron-impact ionization. Their return and rescattering conditions are given by Eqs. (9) and (8), respectively. The yields are then given by

$$\Gamma \sim \int dt' R(t') \delta\left(E_{\mathrm{ret}}(t) - \sum_{j=1}^{2} \frac{[\mathbf{p}_j + \mathbf{A}(t)]^2}{2} - |E_{02}| \right), \qquad (24)$$

where $E_{\mathrm{ret}}(t)$ is the kinetic energy of the electron upon return and the argument in the δ function gives the energy conservation at t. This model is discussed in more detail in [26].

Figure 9 presents the outcome of the classical computation, for the same parameters as in Fig. 1. Interestingly, both figures are very similar. Indeed, there exist only minor differences near the boundaries of the classically allowed region, which occur for high intensities, as displayed in the lower panels of Figs. 1 and 9. Such differences are due to the fact that the yield from the quantum-mechanical computation is exponentially decaying in the region for which electron-impact ionization is classically forbidden, whereas the distribution (24) immediately vanishes. Such discrepancies were also present in the monochromatic case.

Further discrepancies occur for specific phases, in panels (c) and (e) of both figures, and show that the sign reversal starts to take place for slightly smaller absolute phases in the quantum-mechanical case. This effect can be understood if one keeps in mind that the critical phase indicates a change in the dominant set of trajectories, and that prerequisites for this dominance are a large tunneling probability for the first electron and electron-impact ionization being classically allowed. In the particular example provided in the panels (c) and (e) of Figs. 1 and 9, this process has just become allowed for the orbits (7,8), within a small momentum region. In the quantum-mechanical case (Fig. 1), there exist contributions

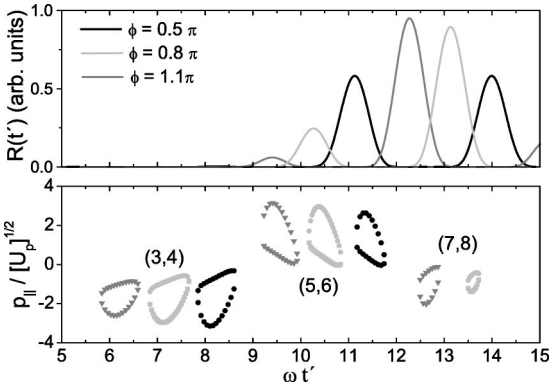

FIG. 10. Quasistatic tunneling rate (23) [panel (a)], together with the classically allowed momenta computed with the classical model [panel (b)], as functions of the tunneling times, for the same parameters as in Fig. 6.

to the yield from near the boundary of such a region, even if rescattering is forbidden, whereas in the classical model (Fig. 9) such contributions vanish. Obviously, such discrepancies are absent in the symmetric momentum distributions obtained in the monochromatic case.

For monochromatic driving fields, a very good agreement has also been reported in previous publications [25,26]. It is not obvious, however, that this would remain true in the few-cycle regime. In fact, apart from yielding distributions which immediately vanish at the boundaries of the classically allowed region, the classical model does not take into account several effects which are present in the quantum-mechanical computation. Examples of such effects are the quantum interference between different possible paths for the returning electron, or the spread of the electron wave packet. Furthermore, the classical model considers an additional approximation with respect to the S-matrix computation, namely Eq. (23), which is a quasistatic, cycle-averaged tunneling rate. This rate is a key ingredient in the distributions given by Eq. (24), and vital for the phase dependence observed in Fig. 9 (cf. Fig. 10 and discussions in [29]). However, its validity may be limited or even questionable in the few-cycle regime. Indeed, recently, a nonadiabatic rate that should be more accurate in this case has been derived [31]. In general, the nonadiabatic rate tends to broaden the time range for which the relevance of sets of orbits persists. We verified, however, that this rate does not modify the yields for the parameter range in question. Discrepancies between the quasistatic and the nonadiabatic rate occur only when the Keldysh parameter $\gamma = \sqrt{|E_{01}|/(2U_p)}$ is much larger than unity. In this case, the driving-field intensity would be far too low for the rescattering process discussed in this paper to be allowed, and thus for the classical model to be applicable. For measurements of NSDI yields below the threshold, see, e.g., Ref. [40].

The subsequent picture (Fig. 10) is the classical counterpart of Fig. 6, providing an interpretation of Fig. 9 in terms of the interplay between the ionization rate (23) and the phase space. Thereby, as in the quantum-mechanical case, we consider parallel momenta along the diagonal $p_{1\|} = p_{2\|} = p_{\|}$ and vanishing transverse momenta. The main contributions

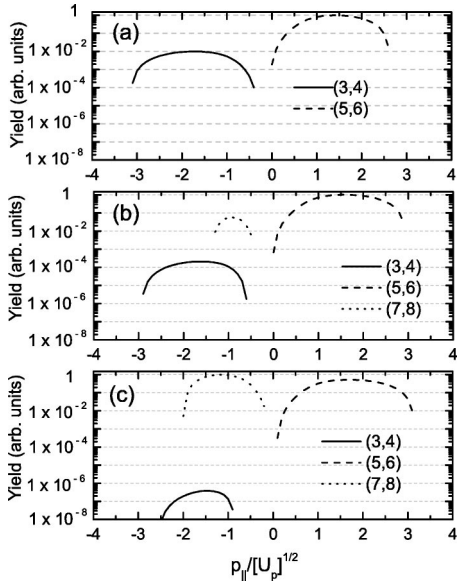

FIG. 11. Individual contributions to the momentum distributions for the same pairs of orbits and for the same parameters as in Fig. 5, computed with the classical model. Parts (a), (b), and (c) correspond to $\phi=0.5\pi$, $\phi=0.8\pi$, and $\phi=1.1\pi$, respectively. The curves have been normalized to the peak value of the largest curve. The contributions from the orbits for which electron-impact ionization is classically forbidden are absent.

to the yield come from pairs of trajectories for which the tunneling probability is large, and for which electron-impact ionization is classically allowed. In the figure, according to such criteria, it is possible to identify two sets of relevant orbits, corresponding to electrons ejected at $9\lesssim\omega t'\lesssim 12$, with positive parallel momenta, and to electrons released at $12\lesssim\omega t'\lesssim 15$, with negative parallel momenta.

According to the absolute phase, similarly to the quantum-mechanical case, there exist three distinct types of behavior. For $\phi<0.8\pi$, apart from the fact that the classically allowed region is almost vanishing for the orbits (7,8), the quasistatic rate (23) is considerably larger for the former set of electrons, so that the distributions are concentrated in the positive momentum regions. Around $\phi=0.8\pi$, such tunneling rates are comparable for both sets of orbits, resulting in nonvanishing yields for positive and negative parallel momenta. Finally, as the phase increases, tunneling is more prominent for the latter set of orbits, and the distributions gradually change towards negative momenta. As in the previous section, the critical phase marks a change in the dominant orbits. This is in agreement with Fig. 6 and with the results in [29].

The ratios between the individual contributions of such pairs of orbits, as well as the momenta for which their maxima occur, displayed in Fig. 11, are also in very good agreement with its quantum-mechanical counterpart (Fig. 5). However, the distributions computed with the classical model are narrower than those obtained using the quantum-mechanical computation. This is once more related to the fact that, in a classical framework, the contributions from the forbidden momentum region cannot be taken into account.

Another interesting feature, which is displayed in Fig. 12, is the existence of other critical phases. For instance, around

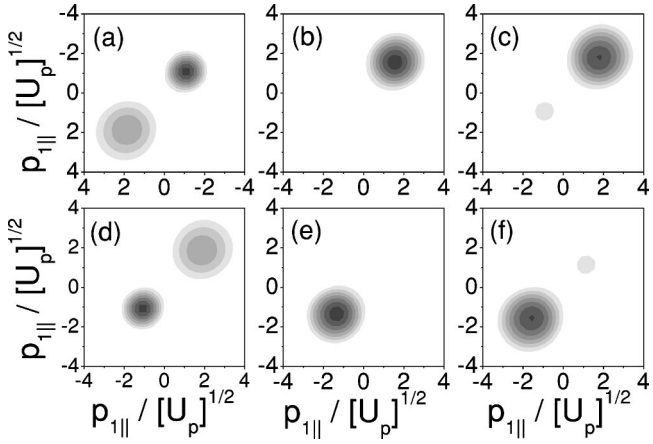

FIG. 12. Differential electron momentum distributions computed with the classical model in Sec. IV for neon subject to a four-cycle pulse ($n=4$) of approximate intensity $I=5.5\times10^{14}$ W/cm^2 ($U_p=1.2$), frequency $\omega=0.057$ a.u., and absolute phases $\phi=0.1\pi$, $\phi=0.5\pi$, and $\phi=0.9\pi$ [panels (a)–(c), respectively], and $\phi=1.1\pi$, $\phi=1.5\pi$, and $\phi=1.9\pi$ [panels (d)–(f), respectively].

$\phi=0.1\pi$, there is a transition in the momentum distributions from the third to the first quadrant in the $(p_{1\parallel},p_{2\parallel})$ plane, i.e., exactly in the opposite direction to the transition in Figs. 1 and 9. Furthermore, the upper and lower panels in Fig. 12 look exactly the same, if the first and the third quadrant are interchanged. This shows that there is a symmetry in the momentum distributions, which is due to the fact that $\mathbf{A}(t,\phi)=-\mathbf{A}(t,\phi\pm\pi)$, so that $|M(p_{1\parallel},p_{2\parallel},\phi)|=|M(-p_{1\parallel},-p_{2\parallel},\phi\pm\pi)|$.

V. CONCLUSIONS

The studies performed in this paper clearly show that nonsequential double ionization with few-cycle pulses is a powerful tool for absolute-phase measurements. More specifically, the yields, as functions of the electron momentum components $(p_{1\parallel},p_{2\parallel})$ parallel to the laser-field polarization, are mainly concentrated either in the positive or negative momentum region, depending on the absolute phase in question. Around a critical phase, such distributions start to shift from one momentum region to the other, until, as the phase increases, complete sign reversal in the momenta occurs. Such features, obtained considering $(e^-,2e^-)$ electron-impact ionization within a quantum-mechanical S-matrix framework, are interpreted in terms of the so-called quantum orbits, which can be directly associated to the trajectories of classical electrons. Both the asymmetry and the critical phase result from the interplay between phase-space effects and the probability that the first electron leaves its parent ion through tunneling ionization. The former and the latter, respectively, determine whether electron-impact ionization is classically allowed or forbidden, or the relevance of a set of orbits to the yield.

The huge effects observed, namely the yields vanishing or appearing over extensive and well-separated regions in the $(p_{1\parallel},p_{2\parallel})$ plane, are due to a particular characteristic of the

rescattering process in question, for which, in addition to a maximal, there is also a minimal classically allowed energy. In other words, electron-impact ionization is allowed only within confined momentum-space regions, defined by the radius in Eq. (10). By varying the driving-field intensity and the absolute phase adequately, this radius can be forced to vanish, so that a whole momentum-space region would become classically forbidden. Furthermore, a particular region can be made irrelevant due to a small tunneling probability for the first electron. This is a major advantage over other phenomena occurring in the context of strong-laser field matter interaction, such as above-threshold ionization and high-order harmonic generation. For both phenomena, there are only maximal classically allowed energies, so that these effects do not occur.

Apart from providing support for previous classical computations [29], the present results allow one to establish a one-to-one correspondence between the classical and the quantum-mechanical approaches.

Tunneling, for instance, is incorporated in the classical model using the quasistatic rate (23) which weighs the electron counts. In the *S*-matrix computation, this process is directly related to the imaginary parts of the start times t'. Both the quasistatic rate and $\mathrm{Im}[t']$ are somehow a measure of the relevance of a set of orbits. Indeed, dominant contributions always come from pairs of orbits for which Eq. (23) is larger or $\mathrm{Im}[t']$ are smaller than those from the remaining pairs. Depending on the absolute phase, this may occur for a single set of orbits, whose contributions lie either in the negative or in the positive momentum regions, or there may be sets of orbits whose contributions compete. A critical phase characterizes a change in the dominant set of orbits.

Furthermore, the phase-space effects which occur if electron-impact ionization becomes classically forbidden, i.e., if the radius in Eq. (10) collapses, are present in both frameworks in very similar, though not entirely identical, ways. In the classical computation, this would lead to vanishing yields, since the condition in the argument of the δ function in Eq. (24) would never be fulfilled. In the quantum-mechanical model, there would be exponentially decaying contributions throughout. If this radius does not collapse, the process will be allowed within a confined momentum-space region. In the classical case, the start and return times coalesce at the boundaries of this region, whereas, quantum mechanically, this does not completely happen.

The above-stated effects explain the minor discrepancies between Figs. 1 and 9. In particular, two types of discrepancies have been observed. First, for high driving-field intensities, the distributions obtained with the quantum-mechanical computation are slightly broader than those from the classical model. Second, in the quantum-mechanical framework, the distributions start to shift at a slightly smaller phase, as compared to the outcome of the classical simulation. The former differences were also present in NSDI with monochromatic driving fields, whereas the latter discrepancies are specific to asymmetric momentum distributions, which occur, for instance, in the context of few-cycle driving pulses.

The agreement between both the quantum-mechanical and the classical computations go beyond the physical explanations for the asymmetry and the critical phase. Indeed, the momentum distributions computed with one or the other method, as well as the predicted critical phase and the interval in which the momenta change sign, are very similar, apart from minor differences near the classical boundaries. This is concrete evidence that the effects reported in this paper are not rooted in a particular model or framework, being, on the contrary, of a deeper physical nature. In fact, recently, a similar asymmetry has been observed in ongoing NSDI experiments with few-cycle driving pulses [41].

ACKNOWLEDGMENTS

Discussions with W. Becker and H. Rottke are gratefully acknowledged. This work was supported in part by the Deutsche Forschungsgemeinschaft (European Graduate College "Interference and Quantum Applications" and SFB407).

[1] M. Lenzner, J. Krüger, S. Sartania, Z. Cheng, Ch. Spielmann, G. Mourou, W. Kautek, and F. Krausz, Phys. Rev. Lett. **80**, 4076 (1998); L. N. Gaier, M. Lein, M. I. Stockman, P. L. Knight, P. B. Corkum, M. Yu. Ivanov, and G. L. Yudin, J. Phys. B **37**, L57 (2004).

[2] T. Brabec and F. Krausz, Rev. Mod. Phys. **72**, 545 (2000).

[3] M. Drescher, M. Hentschel, R. Kienberger, G. Tempea, Ch. Spielmann, G. A. Reider, P. B. Corkum, and F. Krausz, Science **291**, 1923 (2001); P. M. Paul, E. S. Thoma, P. Breger, G. Mullot, F. Auge, Ph. Balcou, H. G. Muller, and P. Agostini, *ibid.* **292**, 1689 (2001); M. Kitzler, N. Milošević, A. Scrinzi, F. Krausz, and T. Brabec, Phys. Rev. Lett. **88**, 173904 (2002); Y. Mairesse, A. de Bohan, L. J. Frasinski, H. Merdji, L. C. Dinu, P. Monchicourt, P. Breger, M. Kovacev, R. Taïeb, B. Carré, H. G. Muller, P. Agostini, and P. Salières, Science **302**, 1540 (2003); R. Kienberger, E. Goulielmakis, M. Uiberacker, A. Baltuska, V. Yakovlev, F. Bammer, A. Scrinzi, T. Westerwalbeslo, U. Kleinberg, U. Heinzmann, M. Drescher, and F. Krausz, Nature (London) **427**, 817 (2004).

[4] M. Hentschel, R. Kienberger, Ch. Spielmann, G. A. Reider, N. Milošević, T. Brabec, P. Corkum, U. Heinzmann, M. Drescher, and F. Krausz, Nature (London) **414**, 509 (2001).

[5] H. Niikura, F. Légaré, R. Hasbani, A. D. Bandrauk, M. Yu. Ivanov, D. M. Villeneuve, and P. B. Corkum, Nature (London) **417**, 917 (2002).

[6] M. Schnürer, Ch. Streli, P. Wobrauschek, M. Hentschel, R. Kienberger, Ch. Spielmann, and F. Krausz, Phys. Rev. Lett. **85**, 3392 (2000); A. Baltuska, Th. Udem, M. Uiberacker, M. Hentschel, E. Goulielmakis, Ch. Gohle, R. Holzwarth, V. S. Yakovlev, A. Scrinzi, T. W. Hänsch, and F. Krausz, Nature (London) **421**, 611 (2003).

[7] A. de Bohan, P. Antoine, D. B. Milošević, and B. Piraux, Phys. Rev. Lett. **81**, 1837 (1998).

[8] E. Cormier and P. Lambropoulos, Eur. Phys. J. D **2**, 15 (1998);

D. B. Milošević, G. G. Paulus, and W. Becker, Phys. Rev. Lett. **89**, 153001 (2002); S. Chelkowski and A. D. Bandrauk, Phys. Rev. A **65**, 061802 (2002).

[9] M. Yu. Kuchiev, Pis'ma Zh. Eksp. Teor. Fiz. **45**, 319 (1987) [JETP Lett. **45**, 404 (1987)]; P. B. Corkum, Phys. Rev. Lett. **71**, 1994 (1993); K. C. Kulander, K. J. Schafer, and J. L. Krause, in *Proceedings of the SILAP Conference*, edited by B. Piraux *et al.* (Plenum, New York, 1993).

[10] G. G. Paulus, W. Becker, W. Nicklich, and H. Walther, J. Phys. B **27**, L703 (1994).

[11] M. Lewenstein, Ph. Balcou, M. Yu. Ivanov, A. L'Huillier, and P. B. Corkum, Phys. Rev. A **49**, 2117 (1994); W. Becker, S. Long, and J. K. McIver, *ibid.* **41**, 4112 (1990); **50**, 1540 (1994); M. Lewenstein, K. C. Kulander, K. J. Schafer, and Ph. Bucksbaum, *ibid.* **51**, 1495 (1995).

[12] P. Dietrich, F. Krausz, and P. B. Corkum, Opt. Lett. **25**, 16 (2000); G. G. Paulus, F. Grasbon, H. Walther, P. Villoresi, M. Nisoli, S. Stagira, E. Priori, and S. De Silvestri, Nature (London) **414**, 182 (2001); G. G. Paulus, F. Lindner, H. Walther, A. Baltuska, E. Goulielmakis, M. Lezius, and F. Krausz, Phys. Rev. Lett. **91**, 253004 (2003).

[13] D. J. Jones, S. A. Diddams, J. K. Ranka, A. Stentz, R. S. Windeler, J. L. Hall, and S. T. Cundiff, Science **288**, 635 (2000); A. Apolonski, A. Poppe, G. Tempea, Ch. Spielmann, Th. Udem, R. Holzwarth, T. W. Hänsch, and F. Krausz, Phys. Rev. Lett. **85**, 740 (2000); A. Baltuska, T. Fuji, and T. Kobayashi, *ibid.* **88**, 133901 (2002).

[14] R. Moshammer, B. Feuerstein, W. Schmitt, A. Dorn, C. D. Schröter, J. Ullrich, H. Rottke, C. Trump, M. Wittman, G. Korn, K. Hoffmann, and W. Sandner, Phys. Rev. Lett. **84**, 447 (2000); Th. Weber, M. Weckenbrock, A. Staudte, L. Spielberger, O. Jagutzki, V. Mergel, F. Afaneh, G. Urbasch, M. Vollmer, H. Giessen, and R. Dörner, *ibid.* **84**, 443 (2000).

[15] B. Feuerstein, R. Moshammer, D. Fischer, A. Dorn, C. D. Schröter, J. Deipenwisch, J. R. Crespo Lopez-Urrutia, C. Höhr, P. Neumayer, J. Ullrich, H. Rottke, C. Trump, M. Wittmann, G. Korn, and W. Sandner, Phys. Rev. Lett. **87**, 043003 (2001); Th. Weber, H. Giessen, M. Weckenbrock, G. Urbasch, A. Staudte, L. Spielberger, O. Jagutzki, V. Mergel, M. Vollmer, R. Dörner, Nature (London) **405**, 658 (2000).

[16] The ponderomotive energy is defined as the time average $U_p = \langle \mathbf{A}(t)^2 \rangle_t / 2$, where $\mathbf{A}(t)$ denotes the vector potential. In this paper, in order to compare our results more directly with the existing literature, we take the expression for U_p in monochromatic driving fields, i.e., $U_p = A_0^2/4$.

[17] See, e.g., R. Dörner, T. Weber, W. Weckenbrock, A. Staudte, M. Hattass, H. Schmidt-Böcking, R. Moshammer, and J. Ullrich, Adv. At., Mol., Opt. Phys. **48**, 1 (2002); J. Ullrich, R. Moshammer, A. Dorn, R. Dörner, L. Ph. H. Schmidt, and H. Schmidt-Böcking, Rep. Prog. Phys. **66**, 1463 (2003) for a review on the subject.

[18] A. Becker and F. H. M. Faisal, Phys. Rev. A **50**, 3256 (1994).

[19] A. Becker and F. H. M. Faisal, Phys. Rev. Lett. **84**, 3546 (2000); **89**, 193003 (2002), and references therein.

[20] J. B. Watson, A. Sanpera, D. G. Lappas, P. L. Knight, and K. Burnett, Phys. Rev. Lett. **78**, 1884 (1997); D. Dundas, K. T. Taylor, J. S. Parker, and E. S. Smyth, J. Phys. B **32**, L231 (1999); W. C. Liu, J. H. Eberly, S. L. Haan, and R. Grobe, Phys. Rev. Lett. **83**, 520 (1999); C. Szymanowski, R. Panfili, W. C. Liu, S. L. Haan, and J. H. Eberly, Phys. Rev. A **61**, 055401 (2000); M. Lein, E. K. U. Gross, and V. Engel, Phys. Rev. Lett. **85**, 4707 (2000).

[21] R. Kopold, W. Becker, H. Rottke, and W. Sandner, Phys. Rev. Lett. **85**, 3781 (2000).

[22] A. Heinrich, M. Lewenstein, and A. Sanpera, J. Phys. B **37**, 2087 (2004).

[23] S. P. Goreslavskii, S. V. Popruzhenko, R. Kopold, and W. Becker, Phys. Rev. A **64**, 053402 (2002); S. V. Popruzhenko, Ph. A. Korneev, S. P. Goreslavskii, and W. Becker, Phys. Rev. Lett. **89**, 023001 (2002).

[24] C. Figueira de Morisson Faria and W. Becker, Laser Phys. **13**, 1196 (2003).

[25] C. Figueira de Morisson Faria, X. Liu, W. Becker, and H. Schomerus, Phys. Rev. A **69**, 021402(R) (2004).

[26] C. Figueira de Morisson Faria, H. Schomerus, X. Liu, and W. Becker, Phys. Rev. A **69**, 043405 (2004).

[27] B. Feuerstein, R. Moshammer, and J. Ullrich, J. Phys. B **33**, L823 (2000); J. Chen, J. Liu, L.-B. Fu, and W. M. Zheng, Phys. Rev. A **63**, 011404(R) (2000); L.-B. Fu, J. Liu, J. Chen, and S.-G. Chen, *ibid.* **63**, 043416 (2001); J. Chen, J. Liu, and S.-G. Chen, *ibid.* **65**, 021406(R) (2002); J. Chen, J. Liu, and W. M. Zheng, *ibid.* **66**, 043410 (2002).

[28] S. L. Haan, P. S. Wheeler, R. Panfili, and J. H. Eberly, Phys. Rev. A **66**, 061402(R) (2002); R. Panfili, S. L. Haan, and J. H. Eberly, Phys. Rev. Lett. **89**, 113001 (2002).

[29] X. Liu and C. Figueira de Morisson Faria, Phys. Rev. Lett. **92**, 133006 (2004).

[30] L. D. Landau and E. M. Lifshitz, *Quantum Mechanics* (Pergamon, Oxford, 1977); M. V. Ammosov, N. B. Delone, and V. P. Krainov, Zh. Eksp. Teor. Fiz. **91**, 2008 (1986) [Sov. Phys. JETP **64**, 1191 (1986)].

[31] G. L. Yudin and M. Yu. Ivanov, Phys. Rev. A **64**, 013409 (2001).

[32] The strong-field approximation mainly consists in neglecting the binding potential in the propagation of the electron in the continuum, the laser field when the electron is bound, or at the rescattering, and the excited states of the atom in question.

[33] L. V. Keldysh, Zh. Eksp. Teor. Fiz. **47**, 1945 (1964) [Sov. Phys. JETP **20**, 1307 (1965)]; F. H. M. Faisal, J. Phys. B **6**, L312 (1973); H. R. Reiss, Phys. Rev. A **22**, 1786 (1980).

[34] R. Kopold, W. Becker, and M. Kleber, Opt. Commun. **179**, 39 (2000); P. Salières, B. Carré, L. Le Deroff, F. Grasbon, G. G. Paulus, H. Walther, R. Kopold, W. Becker, D. B. Milošević, A. Sanpera, and M. Lewenstein, Science **292**, 902 (2001).

[35] In this context, a Stokes transition characterizes a change in the asymptotic expansion of a function. For detailed discussions, see, e.g., R. B. Dingle, *Asymptotic Expansions: Their Derivation and Interpretation* (Academic Press, London, 1973); M. V. Berry, Proc. R. Soc. London, Ser. A **422**, 7 (1989).

[36] C. Figueira de Morisson Faria, H. Schomerus, and W. Becker, Phys. Rev. A **66**, 043413 (2002).

[37] N. Bleistein and R. A. Handelsman, *Asymptotic Expansions of Integrals* (Dover, New York, 1986); H. Schomerus and M. Sieber, J. Phys. A **30**, 4537 (1997).

[38] For neon, there is excellent agreement between computations considering electron-impact ionization and the experimental results, in the long-pulse regime. For other species, such as argon, other physical mechanisms, such as for instance tunneling excitation, may also be important. This issue is discussed

in detail in V. L. B. de Jesus, B. Feuerstein, K. Zrost, D. Fischer, A. Rudenko, F. Afaneh, C. D. Schröter, R. Moshammer, and J. Ullrich, J. Phys. B **37**, L161 (2004).

[39] Specifically for the orbits (1,2), if the first ionization potential vanishes, i.e., in the classical limit, electron-impact ionization is only classically allowed for slightly larger intensities, corresponding to $U_p = 1.218$ a.u., whereas in the *S*-matrix framework, there exist Stokes transitions already for $U_p = 1.2$ a.u.. This is related to the fact that, for (1,2), the driving-field intensity at the tunneling time t' is low enough for the quantum-classical correspondence to become less reliable. This behavior shows that the existence of Stokes transitions is a necessary, but not sufficient, condition for the existence of an energy region for which electron-impact ionization is classically allowed.

[40] E. Eremina, X. Liu, H. Rottke, W. Sandner, A. Dreischuh, F. Lindner, F. Grasbon, G. G. Paulus, H. Walther, R. Moshammer, B. Feuerstein, and J. Ullrich, J. Phys. B **36**, 3269 (2003).

[41] X. Liu *et al.* (unpublished).